

CORONAL MAGNETOGRAPHY OF AN ACTIVE REGION FROM MICROWAVE POLARIZATION INVERSION

B. I. RYABOV¹, N. A. PILYEVA¹, C. E. ALISSANDRAKIS², K. SHIBASAKI³,
V. M. BOGOD⁴, V. I. GARAIMOV⁴ and G. B. GELFREIKH⁵

¹*Institute of Astronomy of the Latvian University, Riga, Latvia*

²*Section of Astrogeophysics, University of Ioannina, 45110 Ioannina, Greece*

³*Nobeyama Radio Observatory, Nagano, Japan*

⁴*Special Astrophysical Observatory RAS, St.-Petersburg, Russia*

⁵*Pulkovo Astronomical Observatory RAS, St.-Petersburg, Russia*

(Received 10 August 1998; accepted 13 October 1998)

Abstract. The microwave circular polarization of the active region (AR) NOAA 7260 on 21–23 August 1992 is analyzed. Two-dimensional images at 1.76 cm with spatial resolution of $\theta = 10''$ from the Nobeyama radioheliograph and one-dimensional scans at 9 wavelengths in the range of 1.81–3.43 cm and $\theta = 16.3''$ – $31.1''$ from the radio telescope RATAN-600 were used. An inversion of the sense of circular polarization through the wavelength range was recorded on 22 August. It is shown that both the wavelength and the time dependence of the inversion are consistent with quasi-transverse (QT) propagation of the radiation in the solar corona. From this, the strength of the coronal magnetic field in the active region was found to be $H = 20$ – 65 G at a height of $h = (5.7$ – $8.7) \times 10^9$ cm above the photosphere on 22 and 30 August and 125 G at the lower height of $(3.7$ – $6.4) \times 10^9$ cm on 23 August. We present a new technique, based on the radio mapping (in both Stokes I and V) of an AR undergoing circular polarization inversion; applying this method to the Nobeyama data we obtained, for the first time, a magnetogram of the coronal magnetic field. For AR 7260 we found values in the range of 70–100 G at heights of $(4$ – $6) \times 10^9$ cm on 23 August, adopting a constant value of $N L_\alpha$ (where N is the electron density and L_α is the scale of the coronal field divergence) of 2.5×10^{18} cm⁻². We compare our results with force-free extrapolations of the photospheric magnetic field from a MSFC magnetogram obtained on 20 August.

1. Introduction

Most of the radio and optical measurements of the coronal magnetic field either integrate along the line of sight or are rough estimates. Radio methods based on the measurement of the characteristics of circular polarization inversion, resulting from the coupling of the electromagnetic modes under quasi-transverse (QT) propagation, are considered to be the only local measurements for the time being. The drawback of these measurements is the fact that the distance between the source of the polarized emission and the coronal region where the coupling occurs is difficult to determine and depends on the coronal structure.

An inversion of the sign of circular polarization of a local microwave source was reported for the first time by Piddington and Minnett (1951). Since then, the inversion has been observed on several occasions, in single-frequency measurements as



a function of time or in spectral-polarization observations through the centimeter range (Peterova and Akhmedov, 1974). It is also quite obvious in two-dimensional maps of high spatial resolution (Kundu *et al.*, 1977; Kundu and Alissandrakis, 1984). The inversion is usually attributed to QT propagation effects in the solar corona.

Both the elaborate theory of the electromagnetic mode coupling in a QT region (QTR) of Cohen (1960) and Zheleznyakov (1970), as well as the increasing resolution of the radio polarization observations permit further refinements in the computation of the coronal magnetic field. Kundu and Alissandrakis (1984), using the dipole approximation for the large scale magnetic structure of an active region (Bandiera, 1982), computed the coronal magnetic field from the displacement of the depolarization line over several days of observations with the WSRT at 6.16 cm. Alissandrakis and Chiuderi Drago (1994) used the Faraday rotation of the plane of linear polarization, detected with a narrow-band receiver, as a diagnostic of the coronal field.

Alissandrakis *et al.* (1996) estimated the coupling parameter at several QT points over an AR and found an agreement between the theory of QT propagation and the extrapolated magnetic field of the AR. The same calculations verified the possibility of a double inversion of the polarization sign along the line of sight. The phenomenon of the double inversion, traced through the centimeter range by spectral-polarization observations with RATAN-600, was reported by Bogod *et al.* (1993a). The double inversion gives the possibility of computing the coronal magnetic field at two QTR points along the same line of sight. Gelfreikh, Pilyeva, and Ryabov (1997) showed that not only the strength, but also the gradient of the field can be computed by means of RATAN-600 one-dimensional scans. The next step for further refinement would be to derive coronal magnetograms from high-resolution radio maps of active region with polarization inversion.

In the present work the evaluation of the coupling parameter and the coronal magnetic field of an AR are made more precise, using the equation derived by Zheleznyakov and Zlotnik (1963), which gives the relation between the degree of circular polarization observed and the coupling parameter. The one-dimensional RATAN-600 scans at 9 wavelengths in the short wavelength range (1 to 18 GHz) of the 'Panoramic Spectrum Analyzer' and the two-dimensional I and V Nobeyama radio maps, with a resolution of $10''$, provide unique information on the strength and structure of coronal magnetic field in ARs. The precise evaluation of the critical wavelength (where the circular polarization is equal to zero) provides a precise radio measurement of the coronal magnetic field. Consequently, the high-resolution radio maps down to wavelengths as short as 1.76 cm ensure the possibility of thorough analysis of the structure of coronal fields of 70–100 G, which have been insufficiently investigated up to now.

The analysis of the polarization inversion in a complex active region (NOAA 7260) was done in the following steps:

– The inversion of the sign of the circular polarization was tested for QT propagation. For this purpose the phenomenological regularities inferred by Peterova and Akhmedov (1974) for the inversion due to QT propagation were applied;

– The value of $H^3 N L_\alpha$ (where H is the strength of coronal magnetic field, N is the electron density, and L_α the field divergence in the coronal QT region) was derived from the observed inversion, on the basis of the QT theory. The position and the shape of the coronal region of the measured $H^3 N L_\alpha$ (i.e., the QTR covering the inverted source) were computed with the help of the extrapolation of the photospheric magnetic field to coronal heights by model dipoles;

– Finally, the position in the corona of the QTR was refined within the frame of the model, by comparison of the simulated inversion with the observed and by correction of the model free parameters.

We also show that the Nobeyama maps of the same AR can provide a coronal magnetogram (a 2-D distribution of the coronal field H on the QTR, projecting on the plane of the sky). The corresponding height of the QT region is inferred from the model. For the sake of comparison with the coronal magnetogram, the results derived from the 1-D RATAN scans and supplemented with the model simulations are presented as 2-D distributions of the AR coronal magnetic field on 22–23 August 1992. In addition, the radio coronal magnetogram is compared with the field extrapolated from a MSFC photospheric magnetogram to coronal heights. In this way we could examine the coronal morphology calculated under the current-free and force-free approximations.

2. Observations

The active region NOAA 7260 was observed with the RATAN-600 from its appearance at the east limb on 11 August to its disappearance at the west limb on 25 August 1992. The intensity and circular polarization (Stokes I and V) were recorded daily at about 09:16 UT with the Panoramic Spectrum Analyzer (Bogod *et al.*, 1993b). For this work we selected data in the short wavelength range (1.71 to 3.43 cm) of the Panoramic Spectrum Analyzer, during 21–23 August, when the active region was approaching the west limb. The east-west (north-south) half-power beamwidth ranges from 16.3'' (11.3') at 1.81 cm to 31.1'' (21.5') at 3.43 cm. Figures 1 and 2 show the RATAN-600 scans, together with the Nobeyama maps for 22 and 23 August.

A set of observations of the AR 7260 in various wavelength ranges (microwave, optical, soft and hard X-rays) was presented at the *Proceedings of Kofu Symposium* (1994) for the days before (17–18 August) and after (24 August) the period analysed here. A description of the observed characteristics of this active region (Leka *et al.*, 1994), as well as a series of investigations on the non-potential configuration in soft X-rays, $H\alpha$ and photospheric magnetograms have also been published (Leka *et al.*, 1996 and references therein).

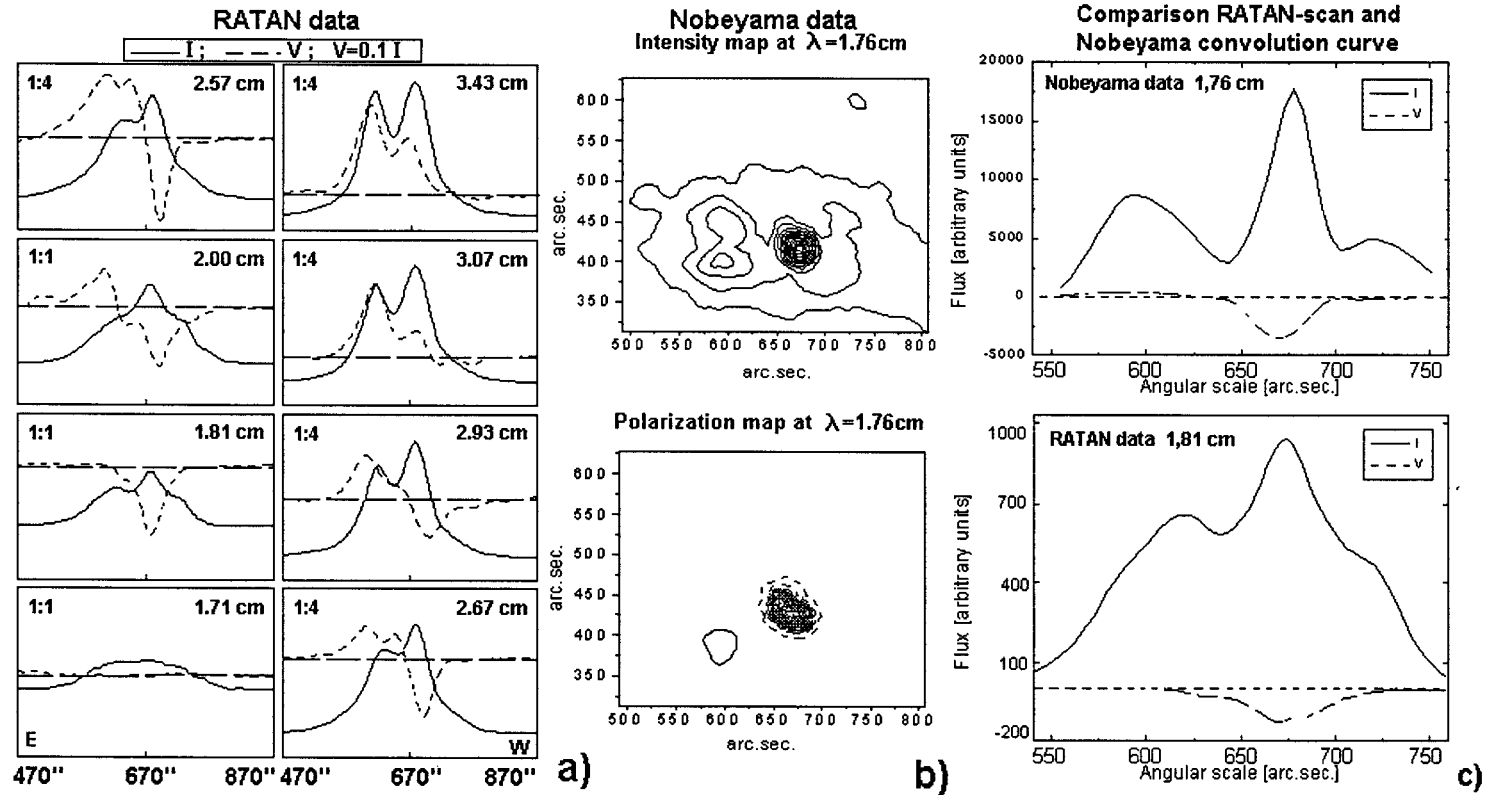


Figure 1. Radio observations of the active region NOAA 7260 on 22 August 1992: (a) RATAN-600 scans in Stokes I (full lines) and V (dashed lines) at 6 wavelengths, taken at 09:16 UT; right-hand circular polarization is positive. (b) Nobeyama radioheliograph 2-D radio maps in I and V at 1.76 cm taken at 02:24 UT; left-hand circular polarization is marked by dashed lines. (c) Comparison of the Nobeyama map convolved with the RATAN-600 fan beam and the 1-D RATAN-600 scan at 1.81 cm. For all plots the position scale starts at the center of the Sun (positive to the west and to the north).

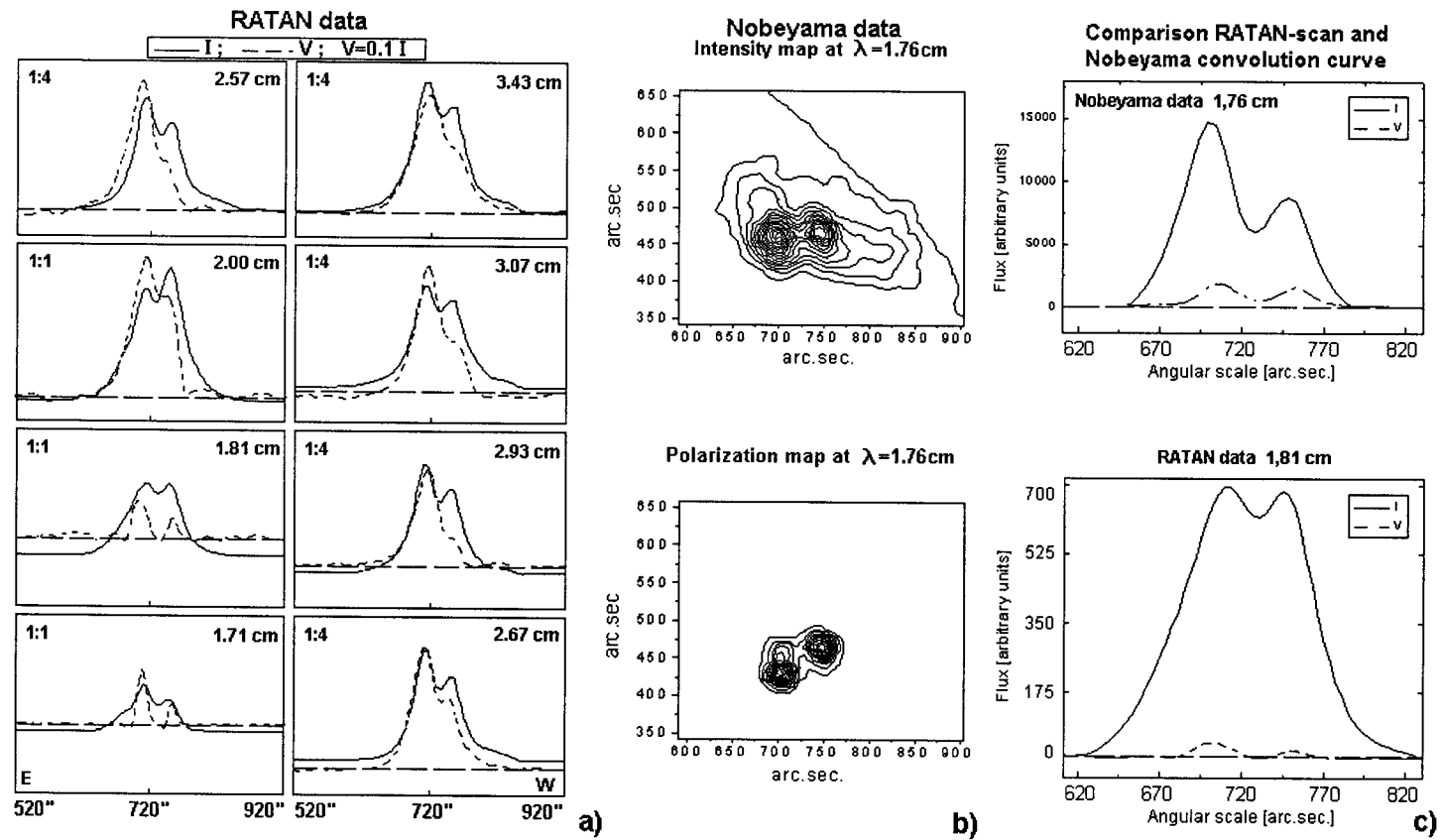


Figure 2. Same as Figure 1 for 23 August 1992.

During its passage across the solar disk, the sunspot group of the region had a large area (half of it in the leading sunspot) and a complex magnetic structure in the photosphere (Figure 4). The characteristics of this active region were a big preceding sunspot (penumbral diameter is 6.2×10^9 cm according to Leka *et al.*, 1994) and fast sunspot growth. In spite of two magnetic δ configurations within the following part of the sunspot group and the large-scale azimuthal twist seen in the magnetograms, only six M-class flares were produced. The peak magnetic field of the main (leading) sunspot was of south polarity and varied from 2400 to 3600 G, according to *Solnechnye Dannye* (1992).

The highest degree of the circular polarization was observed at 2.5 cm and appears to coincide with the sunspot-associated microwave sources. On 21 August the polarization of the western source associated with the dominant leading sunspot was left-handed; the degree of polarization was 15% at 2.0 cm, 25% at 2.57 cm, and 10% at 3.07 cm. The inversion started on 22 August, if we ignore slight variations in the middle of the polarized structure of the AR at 2.28 and 2.94 cm on 21 August. While at 2.93 cm and shorter wavelengths both senses of circular polarization were seen (similar to the structure of 21 August), only right-hand circular polarization was recorded at 3.07 cm and 3.43 cm. This is apparently the result of polarization inversion in the western source, associated with the main sunspot of South magnetic polarity (the prevalence of the extraordinary mode and the corresponding left-handed circular polarization are assumed). On 23 August, right-handed circular polarization dominated over the entire AR 7260 over the entire wavelength range (Figure 2).

The Nobeyama 2-D radio maps show structures similar to the RATAN 1-D scans: on 23 August, the polarization in the western source was inverted at 1.76 cm (Figure 2b). The degree of the circular polarization of the western source dropped from 20% left-hand c.p. on 22 August to 7% right-hand c.p. on 23 August. On 18 August, near the center of the solar disk, the western source was nearly 100% left-hand polarized with the peak brightness temperature 2.2×10^5 K (Shibasaki *et al.*, 1994); this high degree of polarization is a clear evidence that the third harmonic layer was inside the transition region, while the second harmonic was still in the chromosphere.

3. Model Analysis

In order to test whether QT propagation is the origin of the polarization inversion, to evaluate the coronal magnetic field and to estimate the distance of the QT region from the microwave source, we used the model *POLAR2* (Gelfreikh *et al.*, 1987). This model takes into account both the gyroresonance and the bremsstrahlung emission mechanisms and treats properly the quasi-transverse propagation of microwaves in the active region coronal field. The free parameters are determined so

that the computed I and V fit best the observed radio intensity and polarization. A description of the model is given below.

3.1. THE MODEL POLAR2

The absorption coefficient consists of two parts, due to the gyroresonance and the bremsstrahlung processes. The optical depth is integrated along the line of sight, ignoring refraction effects. The gyroresonance emission and absorption are described in terms of the optical depth (Zheleznyakov, 1970) (hereafter all units are in c.g.s.):

$$\tau_{js} \sim \frac{s^{2s}}{2^s s!} N T^{s-1} L_H \lambda f_{js}(H, \alpha), \quad (1)$$

where H is the magnetic field strength, N is the electron density, $s = 1, 2, \dots, 8$ is the number of gyro harmonics, the index $j = 1$ refers to the extraordinary mode and $j = 2$ to the ordinary mode, $f_{js}(H, \alpha)$ is a complicated function of H and α , λ is the wavelength, $L_H = H |dH/dl|^{-1}$ is the scale length of the magnetic field, and α is the propagation angle between \mathbf{H} and the direction of the propagation of microwaves \mathbf{I} . The model under consideration does not integrate N , T , H along the profile of each gyroresonance layer but uses their averaged values within the width of the layer (Zheleznyakov, 1970),

$$L \approx 2.83 L_H \beta |\cos(\alpha)|, \quad (2)$$

of several 10^7 cm. Here $\beta \approx 1.298 \times 10^{-5} T^{1/2}$. The bremsstrahlung absorption coefficient for electrons emitting in the presence of ions under the influence of external magnetic field is (Zlotnik, 1968)

$$\mu_j = Q \lambda^2 N^2 T^{-3/2} B_j(\lambda, N, H, \alpha), \quad (3)$$

where Q is a slowly varying function of N and T , and the function B_j contains the reciprocal of the refractive index $n_j = n_j(\lambda, N, H, \alpha)$.

It is the theory of magnetoionic mode coupling (Cohen, 1960; Zheleznyakov and Zlotnik, 1963) which predicts the transformation of the state of polarization in the layer where the propagation angle $\alpha \approx 90^\circ$. The result, according to Kravtsov and Naida (1976), depends on N , H , and λ , in a layer of width $2(\pi f)^{-1} L_\alpha f_H \approx 10^8$ cm; here $f = c/\lambda$ is the observing frequency, f_H is the gyroresonance frequency, $L_\alpha = \alpha |d\alpha/dl|^{-1}$ is the scale length of magnetic field divergence, and c is the vacuum speed of light.

The model calculates the amplitudes of the extraordinary, c_1 , and the ordinary mode, c_2 , after crossing of the QT layer, from the equations (Zheleznyakov and Zlotnik, 1963)

$$c_1 = C_1 \sqrt{1 - \exp(-2\delta_0)} - C_2 \exp(-2\delta_0), \quad (4)$$

$$c_2 = C_1 \exp(-2\delta_0) + C_2 \sqrt{1 - \exp(-2\delta_0)}, \quad (5)$$

where C_1 , C_2 are the amplitudes of the extraordinary and ordinary mode respectively before they cross the QT layer and δ_0 is the coupling parameter:

$$2\delta_0 \approx 1.15 \times 10^{-25} H^3 N L_\alpha \lambda^4 . \quad (6)$$

The degree of circular polarization is, from Equations (4)–(5),

$$\rho^V = \rho_0^V [-1 + 2 \exp(-2\delta_0)] , \quad (7)$$

where ρ_0^V , ρ^V are the degree of the circular polarization before and after crossing the QT layer respectively.

The brightness temperature in the region above the sunspots was calculated by solving the radiative transfer equation. We used a plane-parallel temperature and density model for the chromosphere–corona transition region and the solar corona at the heights $h > h_0$, in which the conductive flux, F_c , and the gas pressure, P , were assumed constant between the temperature $T_0(h_0) = 10^5$ K and the constant coronal temperature T_c .

Taking into account all these assumptions, a one-parameter model of the atmosphere can be constructed, according to Reimers (1971). The free parameter, Q , is equal to the ratio of the conductive flux of the model to that of a reference atmosphere model: $Q = F_c/F_c^{qs}$. The temperature and electron density for $h > h_0$ are given by (Reimers, 1971)

$$T = T^{qs} \times Q^{2/7} , \quad (8)$$

$$N = N^{qs} \times Q^{5/7} . \quad (9)$$

As a reference atmosphere model, $T^{qs}(h)$, $N^{qs}(h)$, we used the quiet-Sun atmosphere by Borovik *et al.* (1990) with $F_c^{qs} = 2 \times 10^5$ erg cm⁻² s⁻¹, $h_0 = 2 \times 10^8$ cm, and $P_0^{qs}(h_0) = 2 \times 10^{14}$ cm⁻² K (Figure 3).

The coronal magnetic field of the sunspots was simulated by vertical magnetic dipoles, in a manner similar to Sakurai and Uchida (1977) who used solenoids. In rectangular coordinates, centered in an AR with the vertical direction along the z axis, the components of the magnetic field are given by (Oster, 1963)

$$\begin{aligned} H_x &= \sum_{i=1}^N H_i^{ph} z_i^3 \frac{3(x-x_i)(z-z_i)}{2[(x-x_i)^2 + (y-y_i)^2 + (z-z_i)^2]^{5/2}} , \\ H_y &= \sum_{i=1}^N H_i^{ph} z_i^3 \frac{3(y-y_i)(z-z_i)}{2[(x-x_i)^2 + (y-y_i)^2 + (z-z_i)^2]^{5/2}} , \\ H_z &= \sum_{i=1}^N H_i^{ph} z_i^3 \frac{(z-z_i)^2 - 0.5(x-x_i)^2 - 0.5(y-y_i)^2}{[(x-x_i)^2 + (y-y_i)^2 + (z-z_i)^2]^{5/2}} , \end{aligned} \quad (10)$$

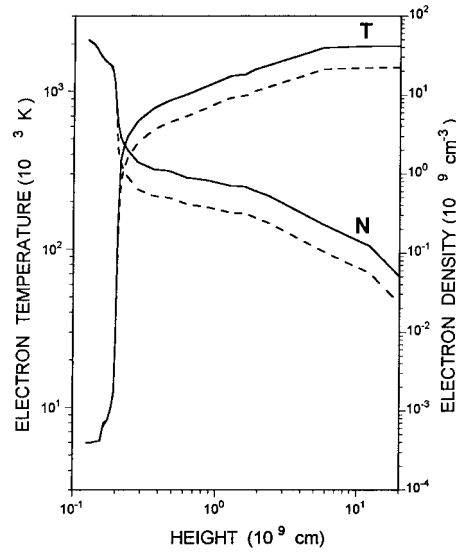


Figure 3. Model distributions of the temperature, T , and the electron density, N , with height, in the quiet-Sun atmosphere (dashed line) and in the active region NOAA 7260 atmosphere (solid line)

where H_i^{ph} is the peak intensity of the i -th photospheric field; x_i, y_i are its rectangular coordinates in the photospheric plane derived from their heliographic coordinates; z_i is the depth of the i -th dipole beneath the photospheric level:

$$z_i = Mk\sqrt{S_i},$$

where S_i is the i th sunspot area in millionths of solar disk units (m.s.d.), and

$$k = \begin{cases} 10^8 \text{ cm msd}^{-1/2} & \text{if } S_i \geq 300 \text{ msd} , \\ 2 \times 10^8 \text{ cm msd}^{-1/2} & \text{if } S_i \leq 70 \text{ msd} \end{cases}$$

(see Akhmedov and Ryabov, 1980, for details); M is a free model parameter. To get the relative magnetic moments of the dipoles, a set of j ($j \geq N$) linear equations are solved for each value of M . Each equation relates the magnetic field H_j^{ph} at the photospheric point x_j, y_j with the superposition of the magnetic fields of appropriately submerged N dipoles.

Taking into account the magnetic field, *POLAR2* is a two-parameter model with one free parameter, Q , related to the gradients of $N(h)$ and $T(h)$ in the chromosphere – corona transition region and the other, M , related to the gradient of an AR magnetic field. The exact value of the parameter T_c is not important because the atmosphere becomes optically thin at these temperatures at short cm wavelengths.

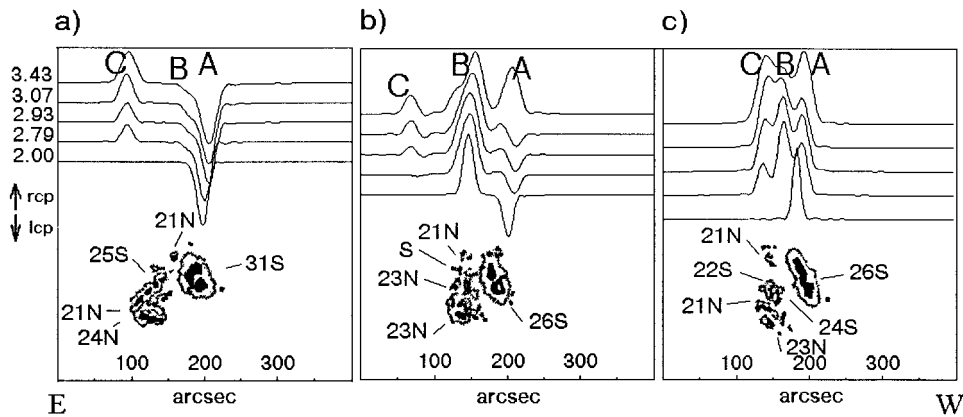


Figure 4. Convolution of the computed V radio maps of the active region NOAA 7260 at 5 wavelengths in the range 2.00–3.43 cm with the RATAN-600 fan beam in arbitrary units on: (a) 21 August; (b) 22 August; and (c) 23 August 1992. The model took into account gyroresonance emission and QT propagation. The sunspot drawings and their peak photospheric magnetic field (in units of 10^2 G) are from the bulletin *Solnechnye Damnye*.

3.2. MODEL COMPUTATIONS

The radio brightness of the AR 7260 was computed at a set of wavelengths taking into account the QT propagation effects. Due to the difference in scale between structures associated with gyroresonance emission in sunspot-associated sources ($\sim 10^8$ cm) and the coronal field governing the sign inversion ($\sim 10^{10}$ – 10^{11} cm), it is possible to determine separately each free parameter of the model. The free parameter M , related with the gradient of coronal magnetic field, affects mainly the sign of the circular polarization, while the free parameter Q , related to the model atmosphere above a sunspot, affects mainly the gyroresonance emission. In this way a distinct and unique model solution can be obtained.

To determine the coronal position of the QTR the model was compared with the RATAN 1-D radio scans. For this purpose a detailed matching with the observed brightness distribution is not necessarily required. The objective of this simulation was to obtain the right sign of circular polarization for any resolved microwave source within the AR in the course of the inversion.

The free parameter Q was chosen so that the observed peak values of the radio brightness in the sunspot sources at 2–3 cm were reproduced. The 2.2×10^5 K brightness of the source associated with the dominant leading sunspot (source A) at $\lambda = 1.76$ cm was reproduced with $Q = 3$, that is $F_c = 6 \times 10^5$ erg cm $^{-2}$ s $^{-1}$, and a coronal temperature $T_c = 1.9 \times 10^6$ K (Figure 3). The size of the model sources was 1.5–2.0 times smaller than that observed at the shorter wavelengths.

The convolution of the computed radio brightness maps with the RATAN-600 beam pattern is shown in Figure 4, for comparison with the observations shown in Figures 1(a) and 2(a). The free parameter M was chosen so that the critical

wavelength, λ_0 , observed in the course of the inversion was such that $\bar{\rho}^V(\lambda_0)$, averaged over the source, was equal to zero.

The depolarization of source *A* on 22 August at $\lambda_0 \approx 3.0$ cm and of source *B* on 21 August at $\lambda_0 \approx 2.8$ cm (Figures 1(a), 4) is represented well by the model with $M = 1.0 - 1.4$ (see Table I). As far as the source *A* on 23 August is concerned, the inversion of the circular polarization sign all over the range 1.8 – 3.5 cm (Figures 2(b) and 4) is simulated with $M = 1.2$ due to a subsequent decrease of the height of the QT region crossed by the microwaves on the next day.

TABLE I
Location and positions of the model dipoles for the AR 7260

Date 1992	Dipole number <i>i</i>	Location	Depth $z_i, 10^9$ cm	Magnetic field* $H_i^{ph}, 10^2$ G	Relative magnetic moment
21 August <i>M</i> = 1.0	1	N15.4 W48.4	2.40	31S	−1.001
	2	N14.0 W36.0	1.60	21N	0.169
	3	N13.0 W37.5	1.60	24N	0.245
	4	N18.0 W36.0	1.10	25S	−0.079
	5	N21.9 W40.8	1.40	21N	0.135
	6	N13.5 W38.5	1.00	16S	−0.063
22 August <i>M</i> = 1.4	1	N15.4 W60.2	3.08	26S	−1.139
	2	N14.0 W51.0	2.17	23N	0.257
	3	N13.0 W52.5	2.17	23N	0.380
	4	N18.0 W49.0	1.26	21S	−0.065
	5	N21.9 W52.8	1.68	21N	0.149
	6	N13.5 W53.5	1.12	16S	−0.066
23 August <i>M</i> = 1.2	1	N15.4 W74.4	2.88	26S	−1.244
	2	N14.0 W64.0	1.92	23N	0.239
	3	N13.0 W65.5	1.92	21N	0.344
	4	N18.0 W62.0	1.08	21S	−0.055
	5	N21.9 W65.8	0.96	21N	0.037
	6	N13.5 W66.5	0.96	24S	−0.071

*Maximum photospheric magnetic field of a model dipole.

3.3. RESULTS

The arched structure of the bipolar ARs gives rise to a QTR. Let us visualize the QTR as an approximately vertical surface bounded by the neutral line of the photospheric magnetic field. The vertical inclination of the QTR depends on (a) the position of an AR on the solar disk and (b) the inclination of the arched structure of the AR coronal magnetic field.

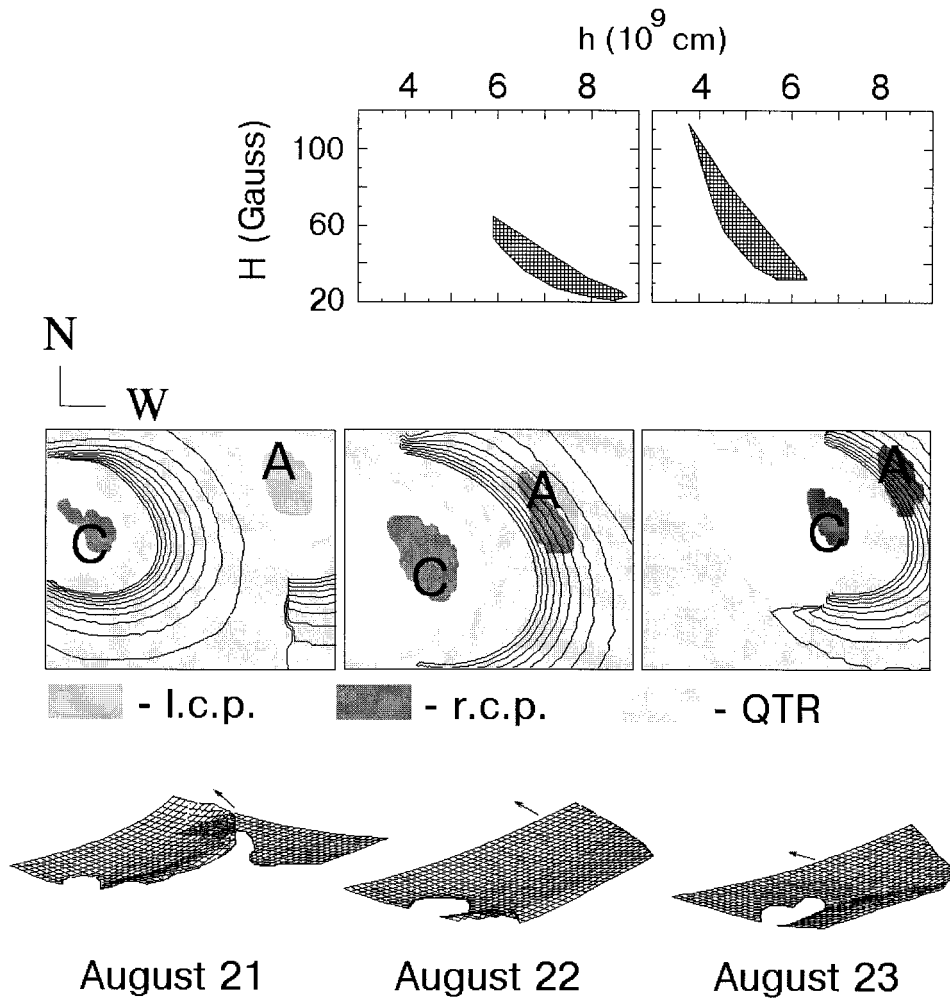


Figure 5. Model computations of the coronal region of quasi-transverse microwave propagation (QTR) (lower row), covering the microwave source A at $\lambda = 3.07$ cm (middle row). Note the polarization inversion in the source A from left-handed (l.c.p.) on 21 August to right-handed (r.c.p.) on 23 August 1992. The source B is outside the frame. Contours of the coronal magnetic field are plotted from 10 to 100 G in steps of 10 G. Upper row: height dependence of the coronal magnetic field in the QTR, which covered source A on 22 and 23 August.

A microwave source associated with the dominant leading sunspot of an AR is covered by the QTR when it is in the western solar hemisphere (see also Bandiera, 1982). The polarization inversion in the source starts at long cm wavelengths and thereafter goes down to the short ones (Figures 1 and 2). This regularity has been shown by the spectral-polarization radio observations of bipolar ARs (Peterova and Akhmedov, 1974). The model simulations with POLAR2 (Ryabov, 1981) show that this regularity is due to the QT propagation. If a dominant sunspot is the leading

one, the height and the coronal magnetic field and the critical wavelength gradually diminish in the QTR. Taking into account Equations (6) and (7), it follows that the shorter the observing wavelength the later the inversion in the leading source occurs.

The inversion manifests itself in a similar way in the complex, non-bipolar, NOAA 7260. Indeed, while the inversion at $\lambda = 4.5$ cm had been considered to start 1–2 days after central meridian passage (CMP) (Peterova and Akhmedov, 1974), the inversion in AR 7260 at the shorter wavelength ($\lambda = 3.07$ cm) occurred 4.5 days after the CMP, on 22 August, 09:16 UT. On the next day, 23 August, the inversion was completed at all the centimeter wavelengths down to $\lambda = 1.76$ cm. The inversion at the early stage was observed on 21 August in the middle of the AR 7260 while on 22 August it shifted to the western part of the AR (Figures 1 and 2).

In particular, as far as the resolved sources *A*, *B*, and *C* are concerned (Figures 4 and 5), we should note that while *A* is obviously associated with the leading sunspot of S magnetic polarity, *B* is apparently the result of integration by RATAN's knife beam over a region with sunspots of both magnetic polarities. Source *C* is apparently associated with the following sunspots, mainly of N magnetic polarity (Figure 4). The most prominent inversion occurred in source *A*. It started on 22 August at the longer wavelengths of 3.45 cm and 3.06 cm and was completed on 23 August at all wavelengths under consideration (Figure 2(b)). According to our model computations, it was on 22 August that the emission from source *A* crossed the QT region with the coronal field strong enough to invert the polarization at wavelengths longer than 3 cm (Equations (6) and (7)).

Figure 5 shows the three-dimensional geometry of the active region. The coronal field in the range of $H = 20$ – 65 G, corresponding to heights of $h = (5.7$ – $8.7) \times 10^9$ cm above the source *A*, is plotted in the middle panels. These values were obtained from the model computations and are consistent with the observed inversion, provided that $N L_\alpha = (1.6$ – $1.7) \times 10^{18}$ cm⁻²; the QTR inclination with respect to the vertical was 39° – 45° . The effective strength of the coronal field, which makes the degree of circular polarization (Equation (7)) exactly equal to zero at $\lambda_0 = 3.07$ cm is 32 G, provided that $N L_\alpha = 1.6 \times 10^{18}$ cm⁻² in Equation (6).

On the next day, that is on 23 August, the line of sight crossed the lower part of the QTR; there the coronal field was strong enough to invert the circular polarization at any centimeter wavelength: 30–125 G, at heights of $(3.7$ – $6.4) \times 10^9$ cm (Figure 5), provided that $N L_\alpha = (2.4$ – $3.0) \times 10^{18}$ cm⁻² and vertical inclination of 35° – 55° .

The polarization of source *C* is not inverted since, being in the western hemisphere and in the trailing part of the active region, it is not covered by the QTR. Both the radio observations of bipolar ARs (Peterova and Akhmedov, 1974) and the model simulations of the QT propagation (Ryabov, 1981) reveal that the microwave source associated with the following sunspots tends to invert the polarization near the east solar limb.

4. Coronal Field Magnetogram

High-resolution maps, such as those of the Nobeyama radioheliograph, provide sufficient information for the measurement of the coronal magnetic field on the QTR. We first note that a value of the magnetic field can be obtained from Equations (6) and (7):

$$H \approx -2.05 \times 10^8 N^{-1/3} L_\alpha^{-1/3} \lambda^{-4/3} \ln^{1/3} \left(\frac{\rho^V / \rho_0^V + 1}{2} \right). \quad (11)$$

Thus the coronal field can be measured above any part of the microwave source where the original degree of circular polarization, ρ_0^V , at the wavelength λ has measurably changed to ρ^V due to the QT propagation in the QTR, provided that N and L_α are known. We note that this method is sensitive to the QT propagation alone and insensitive to the details of the emission mechanism.

For a preliminary analysis we may use a constant value of $N L_\alpha$. A reference value of $N L_\alpha \approx 10^{18} \text{ cm}^{-2}$ is a reasonable estimate, taking into account that the vertical variations of N and L_α are in the opposite sense; this value would result from $N = 10^9 \text{ cm}^{-3}$ and $L_\alpha = 10^9 \text{ cm}$ at the low height of 10^9 cm and $N = 10^8 \text{ cm}^{-3}$, $L_\alpha = 10^{10} \text{ cm}$ higher up at 10^{10} cm . In our case we used a reference value of $N L_\alpha = 2.5 \times 10^{18} \text{ cm}^{-2}$, based on to the model calculations of the previous section. We note that a magnetogram computed in this way can easily be corrected, provided that the precise values of $N L_\alpha$ are known.

In order to apply Equation (11), one should have measurements of both the intrinsic degree of circular polarization, $\rho_0^V(x, y)$, as well as of that after the depolarization effects due to wave propagation, $\rho^V(x, y)$. The former can be obtained from I and V maps on a day without any observable inversion, the latter from maps with clear evidence of inversion. In addition one should choose a suitable region, where the degree circular polarization has changed significantly between the two V maps and the intensity is high enough (e.g., in a sunspot-associated microwave source) to reduce errors and the two maps should be carefully superimposed.

In our case we selected the central part of the microwave source associated with the leading sunspot, shown by a rectangle in Figure 6. The quantity ρ_0^V was computed within the region from the ratio $I(x, y)/V(x, y)$ on 22 August while $\rho^V(x, y)$ was computed from the data of 23 August. In doing so we assumed that there were no propagation effects in the chosen region on 22 August and that $|\rho^V / \rho_0^V| \leq 1$.

The resulting coronal magnetogram is shown in Figure 7(a). We remind the reader that this gives the value of the magnetic field *on* the QT region. The height above the photosphere for each point of this region was deduced from the model calculations of Section 3 and is given in Figure 7(d).

An independent check of the magnetic field can be made from the RATAN-600 data. Starting from $\bar{\rho}^V \approx 0$, we obtain from Equations (6) and (7) that $2 \delta_0 \approx 0.693$ at $\lambda = 3.07 \text{ cm}$. Since the coupling parameter $\delta_0 \sim \lambda^4$, according to Equation (6),

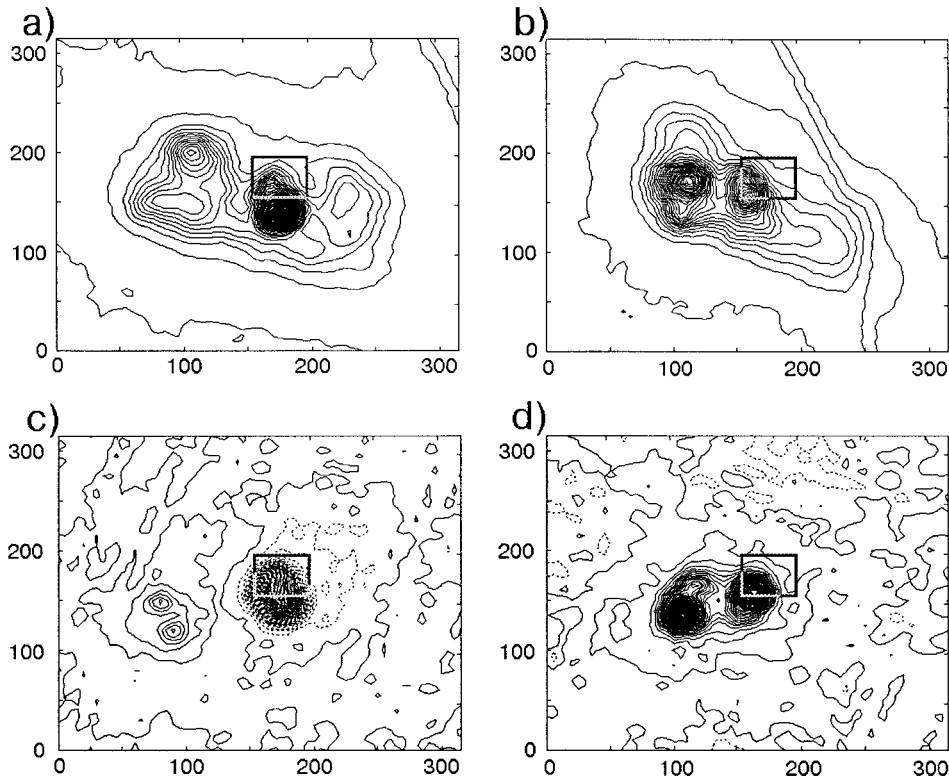


Figure 6. High-resolution maps ($\theta = 10''$) of the active region NOAA 7260 obtained with the Nobeyama radioheliograph at 1.76 cm in intensity (a, b) and circular polarization (c, d) on 22 August (a, c) and 23 (b, d), 1992. The rectangle shows the region ($34'' \times 39''$) selected for the computation of the coronal magnetogram (Section 4).

$2\delta_0 \approx 7.49 \times 10^{-2}$ at the wavelength 1.76 cm of the Nobeyama maps. Hence, the observed degree of circular polarization at $\lambda = 1.76$ cm should be reduced, according to Equation (7), by a factor of $-1 + 2 \exp(-7.49 \times 10^{-2}) \approx 0.856$ on 22 August. Taking into account the time difference between Nobeyama and RATAN-600, this value goes to 0.9. This gives a magnetic field value of 75.3 G, compared to the magnetogram average value of 76.4 G.

The magnetic field on the QT region, computed from the model of Section 3, is shown in Figure 7(b). Although the average value is about the same as that of the coronal magnetogram of Figure 7(a), the structure is smoother and the gradient larger. If we attribute these differences to the variations of the quantity $N L_\alpha$ alone, its values on the QT region can be obtained from Equation (6). They are shown in Figure 7(c), ranging from $(0.5-15) \times 10^{18} \text{ cm}^{-2}$.

More realistic than the dipole superposition is the extrapolation based on photospheric magnetograms. Figure 8(a) shows a magnetogram of NOAA 7260 observed at the Marshall Space Flight Center on 20 August 1992 (angular resolution $3.2''$);

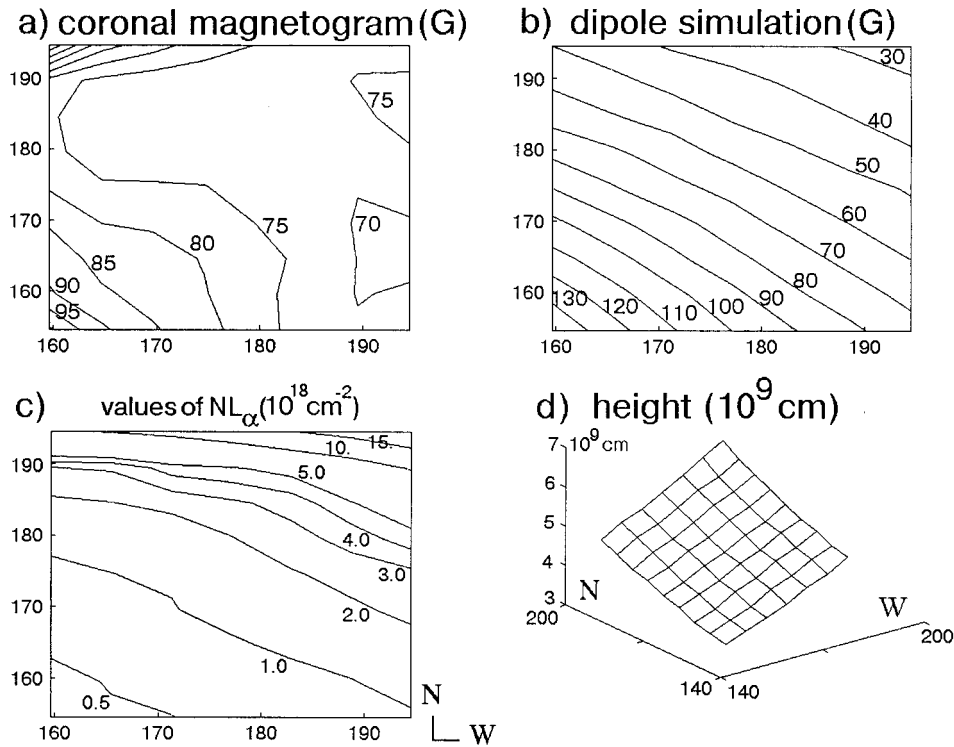


Figure 7. Coronal magnetograms of NOAA 7260 on 23 August 1992: (a) deduced from the Nobeyama radioheliograph maps, for $N L_{\alpha} = 2.5 \times 10^{18} \text{ cm}^{-2}$ (Section 4) and (b) on the basis of the magnetic field model obtained from the RATAN-600 spectral polarization observations (Section 3.3). (c) shows a map of the values of $N L_{\alpha}$, obtained by comparing (a) and (b); (d) shows the height of the coronal region of QT propagation.

unfortunately no observations were available for 21–23 August. From this magnetogram we computed the coronal magnetic field using the constant- α force-free algorithm of Alissandrakis (1981). For the sake of comparison with the coronal magnetogram, the heights of the QT region for 23 August were used (Figure 8(b)). The value of α was varied in the range given by Leka *et al.* (1996) for the leading sunspot: -2×10^{-10} to $-3 \times 10^{-9} \text{ cm}^{-1}$.

In comparing the extrapolated field of Figures 8(c) and 8(d) with the coronal magnetogram (Figure 7(a)), one should take into account the decrease of the photospheric field of the sunspot from 20 August to 23 August (see Table I). Unlike the field derived from the superposition of a few dipoles, the extrapolated coronal field does reproduce reasonably well the local minimum seen in the coronal magnetogram. The field morphology at $h = 4\text{--}6 \times 10^9 \text{ cm}$ strongly depends on the value of α . The best fit to the coronal magnetogram is for $\alpha = -10^{-9} \text{ cm}^{-1}$.

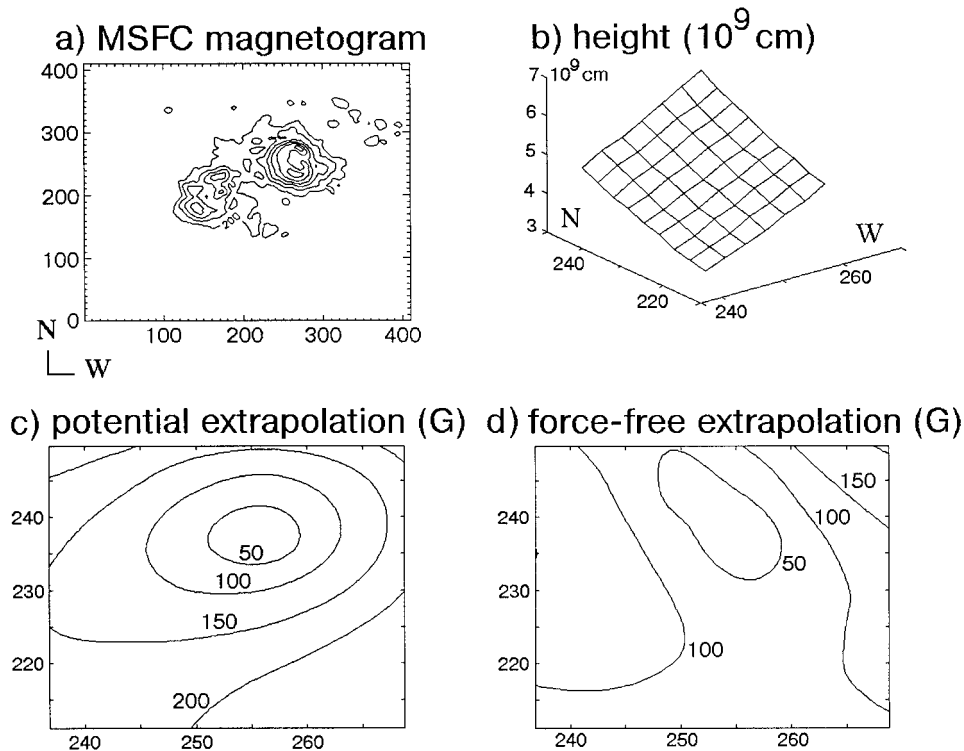


Figure 8. (a) A photospheric magnetogram of NOAA 7260 from the Marshall Space Flight Center (intensity of vector field) on 20 August 1992; (c) potential and (d) force-free ($\alpha = -10^{-9} \text{ cm}^{-1}$) extrapolations at the height of the QT region; (b) shows the height of the QT region, assumed to be the same as for 23 August (Figure 7(d)).

5. Summary and Discussion

The combined observations of the RATAN-600 radio telescope and the Nobeyama radioheliograph gave us the opportunity to make an in-depth study of the characteristics of circular polarization inversion and to model it in terms of the magnetic field on the corona above an active region approaching the west limb. It was easy to trace the polarization inversion of the western sunspot-associated source both through wavelength (Figure 1(a)) and in the course of time (Figures 1 and 2).

The analysis of the polarization inversion gave the following results:

(1) We confirmed that QT propagation of microwaves in the solar corona is the principal cause of inversion of the sign of circular polarization. The original circular polarization was assumed to be due to the extraordinary mode prevalence in a unipolar magnetic field. The observed features, namely the start of the inversion on 22 August at long wavelengths and its completion at 23 August at wavelengths as short as 1.76 cm, were characteristic of QT-propagation effects in the emis-

sion of a leading, sunspot-associated source, near the western limb (Peterova and Akhmedov, 1974; Alissandrakis *et al.*, 1992).

(2) The model computations of the QT propagation of circularly polarized emission fit well the observed features of the circular polarization on 22 August 1992, in the course of the inversion (cf. Figures 1(a), 2(a) and Figures 4(b), 4(c)). From this model and the theory of electromagnetic mode coupling in a QT region, the coronal magnetic field in the AR 7260 was computed: $H = 20\text{--}65$ G at $h = (5.7\text{--}8.7) \times 10^9$ cm on 22 August and $30\text{--}125$ G at lower heights of $(3.7\text{--}6.4) \times 10^9$ cm on 23 August. This field overlies the leading sunspot of the AR, with peak photospheric field of $2600\text{--}3300$ G.

The values of the magnetic field derived here are higher than those obtained from polarization inversion data at 6.16 cm by Kundu and Alissandrakis (1984) and Alissandrakis *et al.* (1996), which were in the range of $10\text{--}20$ G. This is not surprising, since the inversion at longer wavelengths occurs higher up in the corona ($h \sim 10^{10}$ cm).

(3) We propose a new technique for computing coronal magnetograms, based on radio maps in I and V Stokes parameters and applied it in observations with the Nobeyama radioheliograph at 1.7 cm (Figures 6, 7(a)). The average value of the magnetic field intensity on the QT region measured in this way was 76 G on 23 August. This measurement assumed a constant value of $N L_\alpha = 2.5 \times 10^{18}$ cm $^{-2}$. The height of the QT region, $(4\text{--}6) \times 10^9$ cm above the photosphere, was deduced from the model computations.

(4) The coronal magnetogram was compared with the extrapolated photospheric field, under the potential and the force-free assumption, from a MSFC magnetogram obtained on 20 August. Since this was three days earlier than the coronal magnetogram, only the morphology of extrapolated and measured coronal field was compared. Shibasaki *et al.* (1994) and Leka *et al.* (1996) reported evidence for strong currents in the magnetosphere of NOAA 7260. The best fit to the coronal magnetogram was for $\alpha = -10^{-9}$ cm $^{-1}$, which is within the range estimated by Leka *et al.* (1996): $\alpha = -2 \times 10^{-10}$ to -3×10^{-9} cm $^{-1}$. Moreover, the structure of the coronal magnetic field deduced from the radio maps, which includes a local minimum, resembles that of the extrapolated photospheric field above leading sunspot.

The analysis of the polarization inversion is a good example of what can be done by joint observations with the radiotelescope RATAN-600 and the Nobeyama radioheliograph. RATAN-600 is better suitable for the inversion diagnostics due to its spectral-polarization capabilities, while the Nobeyama radioheliograph can supply coronal magnetograms of high resolution.

Acknowledgements

The authors wish to thank M. Hagyard (Marshall Space Flight Centre) for supplying the magnetogram and A. N. Korzhavin (Special Astrophysical Observatory)

for his assistance. This research has been partially supported by INTAS grant 94-4625, Russian Fund for Basic Research (RFBR) Projects 96-02-16598a and 96-02-16268a, ISF grant LFB 000, grant LJB 100 from the Joint Program of the Government of Latvia, and a grant from the Greek General Secretariat for Research and Technology.

References

- Akhmedov, Sh. B. and Ryabov, B. I.: 1980, *Solnechnye Dannye* No. 12, 85.
- Alissandrakis, C. E.: 1981, *Astron. Astrophys.* **100**, 197.
- Alissandrakis, C. E. and Chiuderi Drago, F.: 1994, *Astrophys. J. Lett.* **428**, L73.
- Alissandrakis, C. E., Lubyshev, B. I., Smolkov, G. Ya., Krissinel, B. B., Treskov, T. A., Miller, V. G., and Kardapolova, N. N.: 1992, *Solar Phys.* **142**, 341.
- Alissandrakis, C. E., Borgioli, F., Chiuderi Drago F., Hagyard M., and Shibasaki, K.: 1996, *Solar Phys.* **167**, 167.
- Bandiera, R.: 1982, *Astron. Astrophys.* **112**, 52.
- Bogod, V. M., Gelfreikh, G. B., Ryabov, B. I., and Hafizov, S. R.: 1993a, *The Magnetic and Velocity Fields of Solar Active Regions*, in Harold Zirin, Guaxiang Ai, and Haimin Wang (eds.), ASO Conference Series, Vol. **46**, p. 302.
- Bogod, V. M., Vatrushin, S. M., Abramov-Maximov, V. E., Tsvetkov, S. V., and Dikij, V. N.: 1993b, in Harold Zirin, Guaxiang Ai, and Haimin Wang (eds.), *The Magnetic and Velocity Fields of Solar Active Regions*, ASP Conference Series, Vol. 46, p. 306.
- Borovik, V. N., Kurbanov, M. Sh., Livshits, M. A., and Ryabov, B. I.: 1990, *Soviet Astron.* **34** (5), 522.
- Gelfreikh, G. B., Peterova, N. G., and Ryabov, B. I.: 1987, *Solar Phys.* **108**, 89.
- Gelfreikh, G. B., Pilyeva, N. A., and Ryabov, B. I.: 1997, *Solar Phys.* **170**, 253.
- Kundu, M. R. and Alissandrakis, C. E.: 1984, *Solar Phys.* **94**, 249.
- Kundu, M. R., Alissandrakis, C. E., Bregman, J. D., and Hin, A. C.: 1977, *Astrophys. J.* **213**, 278.
- Leka, K. D., Canfield, R. C., McClymont, A. N., and Van Driel-Gesztelyi, L.: 1996, *Astrophys. J.* **462**, 547.
- Leka, K. D., Van Driel-Gesztelyi, L., Nitta, N., Canfield, R. C., Mickey, D. L., Sakurai, T., and Ichimoto, K.: 1994, *Solar Phys.* **155**, 301.
- Peterova, N. G. and Akhmedov, Sh. B.: 1974, *Soviet Astron.* **17**, 768.
- Piddington, J. H. and Minnett N. C.: 1951, *Australian J. Sci. Res.* **A4**, 131.
- Proceedings of Kofu Symposium*: 1994, S. Enome and T. Hirayama (eds.), NRO Report No. 360.
- Reimers, D.: 1971, *Astron. Astrophys. Suppl.* **14**, 198.
- Ryabov, B. 1981, *Issled. Sol. Krasn. Zvezd* **15**, 5.
- Solnechnye Dannye*: 1992, No. 8.
- Sakurai, V. and Uchida, Y.: 1977, *Solar Phys.* **52**, 397.
- Shibasaki, K., Irimajiri, Y., Leka, K. D., and Canfield, R. C.: 1994, *Publ. Astron. Soc. Japan* **46**, L17.
- Zheleznyakov, V. V.: 1970, *Radio Emission of the Sun and Planets*, Oxford, Pergamon Press, Oxford.
- Zheleznyakov, V. V. and Zlotnik, E. Ya.: 1963, *Astron. Zh.* **40**, 633.
- Zlotnik, E. Ya.: 1968, *Astron. Zh.* **45**, 310.